APPENDIX E

DETAILED ASSESSMENT OF THE PHASE 2 PRELIMINARY FIELD TRIAL RESULTS

CONTENTS

E.1 INTRODUCTION

Ground penetrating radar results are presented as radargram time sections which have one axis being distance along the traverse the other being two-way-travel-time measured in nanoseconds (ns). These time sections can be converted into depth sections if the electromagnetic wave velocity of the medium being investigated is known. Thus depths to reflectors interpreted from the time sections can be calculated. The accuracy of the depth calculation is dependent on how realistic a velocity is used together with the resolution of the antenna. Different material layers will have a different velocity and thus a composite velocity calculation should theoretically be made. The contractors in Phase 2 used a "bulk" or "average" velocity which they applied to the whole time section.

Resistivity imaging results are presented as true iso-resistivity versus depth sections in ohm - meters (Ωm). The resistivity values calculated from the raw data is an apparent resistivity related approximately to depth. This data is then modelled using inversion software to produce true iso-resitivity depth sections. Different contouring packages have been used to present the data which account to some extent for the variability in the styles of presentation between different contractors.

Iso-conductivity maps have been produced to present the FDEM data in milli-Seimens per meter (mS/m). Measurements were generally taken on a 1m grid over the slope and the results simply contoured with little data processing. Both in-phase and conductivity are presented results (see Appendix B).

SASW results are presented as pseudo-dispersion curves and shear wave velocity depth profiles by IGGE and GSC.

E.2 RESULTS FROM SITE E

Figure E1 presents two radargrams made along the vertical traverse TE01 at site E (Figure 12). Figure E1a was produced by GA and E1b was produced by IGGE. Both radargrams have been produced using 500MHz antennas and essentially the same equipment (GA used the SIR 2 system and IGGE used the SIR 10 system). The GA radargram is presented in grey scale with wiggle trace superimposed, the lighter grey tone and higher amplitude wiggles indicating a high energy/amplitude reflection. The IGGE radargram is presented as a wiggle trace only. In Figure E1a three zones of different reflection characteristics and energy have been identified on the radargram: zone 1 is characterised by parallel sets of low energy reflectors, zone 2 is characterised by poorly defined reflectors and zone 3 by well defined high energy reflectors which appear to be located directly above each tie beam. The limit of penetration is about 55ns. The three well-defined zones are not evident on Figure E1b. However, zones of higher energy reflectors do occur above each tie beam between 9ns to 40ns which compared to the GA radargram would put them in zone 2 rather than zone 3.

Figure E2 presents two radargrams also made along traverse TE01 produced using 100MHz antennas. Figure E2a was produced by GSC and E2b was produced by IGGE. Although identical equipment has been used, GSC carried out the radar survey by moving the radar antenna point by point along the traverse at 0.25m intervals in order to stack the radar

signal to improve the signal to noise ratio. IGGE carried out the radar survey in continuous mode where the antenna is moved at a constant rate along the traverse. Both radargrams are presented as wiggle traces. It should be note that on both radargrams the time scale is over 100ns whereas the radargrams on Figure E1 the time scale was between 40ns and 50ns. In Figure E2a the contractor has interpreted a stepped wall profile with increases in wall thickness coinciding with each tie beam. The series of parallel reflectors within the first 25ns are direct wave events and not real reflectors. A high-energy reflector parallel to the wall face is evident at 25ns but only the top 2m has been interpreted as being significant. Other intermittent high energy reflectors are evident in the radargram. At two-way travel times greater than about 90ns the reflected events are obscured by noise and gain-controlled artefacts which manifest themselves as parallel, equally-spaced high-energy events on the radargram. The first of these artefacts has been interpreted by GSC as the interface between fill and highly decomposed rock (Figure E2a). The same reflectors are not evident on Figure E2b; however the three zones of high energy reflectors located above each tie beam at about 50ns agree well with the similar reflectors in zone 3 of the GA 500MHz radargram (Figure E1a). Reflection events are obscured by noise at two-way travel times greater than about 75ns on Figure E2b.

Figures E1 and E2 demonstrate the following points;

(i) the penetration depth of 500MHz antenna is approximately 50ns,

(ii) the noise to signal ratio can be improved and hence depth of penetration by stacking,

(iii) different contractors produce different radargrams using the same equipment, and

(iv) gain controlled artefacts were interpreted as real reflectors by several contractors.

Figure E3 presents three iso-resistivity sections made along TE03 at site E (Figure 12). These are horizontal sections through the wall orientated with east to the left which is the high part of the wall. All three sections have a zone of high resistivity of greater than about 400Ωm which extends to a depth of 3m in the east and thins westwards to approximately 2m. This high-resistivity zone has been interpreted as the masonry wall by each contractor. A sharp decrease in resistivity is seen behind the wall. There are also some similarities in the details of the sections, especially Figures E3a and E3b produced by GA and FGS respectively. Two resistivity lows can be identified within the zone of high resistivity, one centred at about 10m on both sections and another which extends from 14m to 21m on Figure E3a and from about 15m to 18m and at 20m on Figure 18b. These zones are not observed on Figure 18c produced by BS. Low-resistivity values (less than 100Ωm) are shown on Figure E3c running the full length of the wall, extending from the face to about 0.5m into the wall. It is considered unlikely that this low-resistivity zone is real since the wall facing is composed of slightly decomposed granite blocks which should have a resistivity greater than 400Ωm. The low-resistivity zones identified on Figures E3a and E3b were interpreted by GA as associated with zones of high moisture content within the wall which corresponded with seepage from weepholes (Figure 12). A parallel traverse 3.5m above

TE03 carried out by GA also show the same pattern of low resistivity. FGS did not comment on the zones of low resistivity.

These examples demonstrate that:

(a) the general characteristics of the iso-resistivity depth sections produced by different contractors are similar even though different equipment, electrode spacing, electrode type and inversion software has been used;

(b) the detail contained in each section can differ and is probably related to some extent to the contouring package used, and

(c) the interpretation of anomalies is dependent on the experience of the geophysicist.

E.3 RESULTS FROM SITE F

The geophysical results and interpretation presented in this section were all made by GA and are used to demonstrate the information which may be gained from a combined GPR and RI survey. Only the key information which supports the interpretation contained in the GA report is presented. For more details the contractors final interpretative report should be consulted (Golders, 1997). Two horizontal radargrams made along TF02 (Figure 13) using a 500MHz and a 100MHz antenna are presented in Figure E4. The 0m chainage is located at the south eastern end (Figure 13). The 500MHz radargram is presented in grey scale and the 100MHz radargram in grey scale with a wiggle trace overlay. The first obvious feature, which shows up best in the 500MHz data, is the zone of subdued reflectors starting at chainage 21m. This has been attributed to conductive soils such as clay fill directly behind the masonry wall which attenuate the radar waves and reduce penetration. This change in the radargram coincides with the change in masonry wall height. The wall is interpreted to be about 1m thick along this section assuming an electromagnetic wave velocity of 0.122m/ns. From 0m to 21m the 500MHz radargram is characterised by many parabolic reflectors. Close inspection of the data reveal several features: a change in signal character at about 36ns suggesting a change in the material type, intermittent coherent reflectors occur at this two-way travel time in the 100MHz radar data, and a zone of less pronounced parabolic reflectors between chainage 12m and 17m. Preliminary interpretation of these features are that the bright parabolic reflectors represent individual masonry blocks within the wall, possibly with associated voids, the change in nature of the reflectors at 36ns could be the back of the wall (at 2m assuming a velocity of 0.122m/ns), and the zone of less-pronounced reflectors represents an area within the wall with less voids between each masonry block.

Two inverse modelled resistivity sections are shown on Figure E5. The lower was made along TF02, the upper along a parallel traverse about 2m above TF02. Both sections have a zone of high resistivity of greater than about 400Ωm which extends to a depth of between 2.5m and 3.2m. From chainage 22m this zone reduces in depth to about 1m along TE02 (note that the upper section does not extend into the lower part of the wall). This high resistivity zone has been interpreted as being the masonry wall. The reduction in wall thickness at chainage 21m agrees

well with the GPR results and the change in wall height. However, GA suggest that this could also be due to geometrical effects and possible short circuiting as the top of the wall beyond chainage 21m is closer to the traverse. The geometrical effect could also explain the apparent gradual thinning of the wall to the south east from about chainage 4m due the presence of the stair case. However, the wall may thin in this area since the stair case would add to the stability of the wall above it.

Two zones of relatively higher resistivity can be observed in the section TF02 from chainage 4m to 15m and from 17m to 22m. These are interpreted by GA as zones of higher void content and generally correspond to the areas of bright parabolic reflectors in the GPR data. The area of lower resistivity from 15m to 17m roughly corresponds to the zone of less pronounced reflectors in the GPR data and supports the interpretation of a low-void zone within the wall (air has a very high resistivity compared to rock). The upper section also contains a zone of high resistivity but of limited extent, which suggests that the lower part of the wall has more voids than the upper part.

The preliminary interpretation made by GA showing the various anomalous areas within the wall is presented on Figure E6. The geophysical interpretation suggests that the wall has essentially three different characteristics: areas with many voids characterised by zones of high resistivity and bright parabolic GPR reflectors, areas with less voids characterised by lower resistivity and less pronounced GPR reflectors (which appear to be located around the part of the wall containing the weepholes), and an area where the wall is thinner with conductive material behind characterised by zone of poor GPR penetration. Based on this interpretation, horizontal drillholes were located within the three zones (Figure 13). The GI generally confirmed this interpretation. The findings of the GI are described in Section 4.4.3 and a section through the wall is shown on Figure 18. The area of many voids appear to correspond with areas of the wall composed of cobbles and boulders of partially weathered rock without any mortar infill, whilst the zone of less voids appear to coincide with an area of wall composed of mass concrete. The GI confirmed that wall thickness reduces to 1.5m (Figure 19) at chainage 21m and has clay fill behind its rear face.

E.4 RESULTS FROM SITE G

Iso-conductivity maps produced by GA and FGS are presented on Figures E7 and E8 respectively. GA used a Geonics EM-38 conductivity meter which has a depth range of about 2m whilst FGS used a Geonics EM-31 conductivity meter which has a depth range of about 5m. The GA map is therefore showing responses to near surface changes in conductivity whilst the FGS map is showing responses to deeper changes in conductivity. However, the larger EM-31 should also be influenced to a greater extent than the EM-38 by cultural interference since boom length and therefore zone of influence is much greater (see McDowell (1981) referenced in Appendix B). Both iso-conductivity maps have large high conductivity anomalies running along the toe of the slope. These are probably associated with services located within the pavement and the metal safety barrier erected along the slope toe. It is worth noting that higher conductivities were recorded by the EM-31. Other conductivity highs are associated with the Towngas pipe running up the slope along the western boundary. This anomaly was only observed by the EM-38. Conductivity lows associated with a concrete drainage gully and a concrete-filled pipe are also shown by the EM-38 (Figure E7). The pipe anomaly is also picked

up by the EM-31 (Figure E8). The conductivity of the rest of the slope generally falls between 8 and 20 mS/m. A change in conductivity is evident across the middle portion of the slope as shown on Figure E7, but this change is not seen in the EM-31 data. The variation across the slope could be due to subtle changes in moisture content of the near-surface materials, changes in the chunam, or subtle changes in the geology across the slope. This change in conductivity appears to have been masked by cultural anomalies along the toe and north west edge of the slope and was not observed by the EM-31. Both conductivity meters were affected by cultural objects. The EM-38 appears to be effected more by surface objects as compared to the EM-31, which had larger anomalies associated with buried services and metallic safety fences remote from the survey location. The GI did not identify any geological or man-made feature which could explain the change in conductivity across the slope recorded by the EM-38

E.5 RESULTS FROM SITE H

Four contractors carried out SASW at the fill slope (see Appendix C). However, only BS, GSC and IGGE present the results in their preliminary report. Both GSC and IGGE present wave velocity versus depth curves together with shear wave velocity-depth sections derived from these curves. An example of the wave velocity versus depth curves is shown on Figure E9. The depth element is only approximate and has been estimated as being half the appropriate wavelength for a specific velocity. This is a crude method of depth calculation and does not conform to the methods recommended by Stokoe et al (1994) (see Appendix B). The velocity versus depth curves presented by GSC and IGGE are therefore effectively dispersion curves (velocity versus wavelength) and are termed pseudo-dispersion curves in this report. The pseudo-dispersion curves shown on Figure E9 are complex and it is likely that the coherence value, which is an indicator of the quality of the data at various frequencies, is less than one (Stokoe et al, 1994) for most of the data. For instance, the pseudo-dispersion curve at 4.5m shown on Figure E9 indicates that the wavelength equivalent to a depth of 4m has at least four corresponding velocities, which is uninterpretable. The velocity-depth sections produced from these pseudo-dispersion curves are therefore not reliable and cannot be used with any confidence. There is also no consistency between the IGGE and GSC velocity-depth sections.

BS present SASW data in a different form which also does not conform to the methods recommended by Stokoe et al (1994). BS plot wavelength, frequency and acceleration against chainage along a particular traverse. Some qualitative interpretation is then made regarding the nature of the near surface materials along the traverse line based on the measured surface wave values.

GA present dispersion curves for the site in their final interpretative report (Golder Associates, 1997) and state that the coherence value is very low for the results at the site, probably due to the heterogeneous nature of the fill.

There does not seem to be a universally-accepted method of carrying out the SASW, which makes it difficult to directly compare between the different contractors results. However, the dispersion curves presented by GA and the pseduo-dispersion curves presented by IGGE and GSC do exhibit the same low coherence values, which is probably due to the heterogeneous nature of the fill at the site as confirmed by the GI.

LIST OF FIGURES

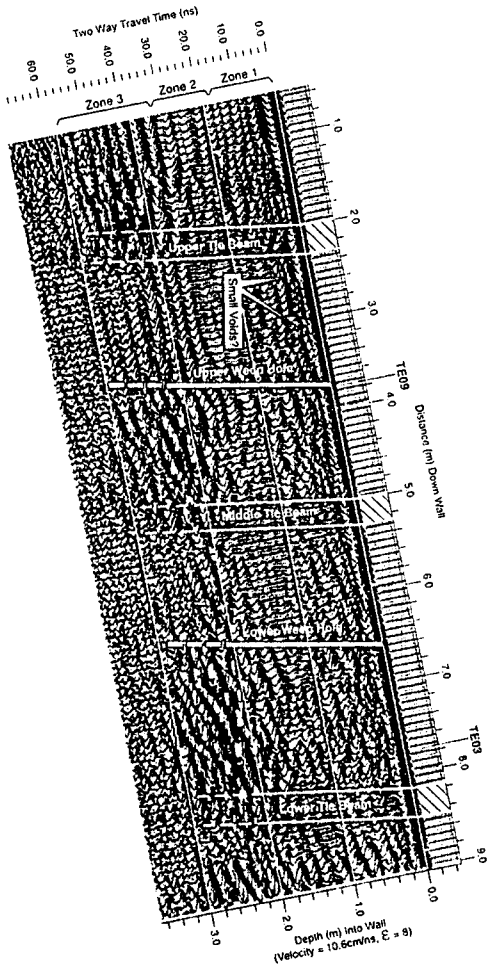

E1a - After Golders (1996b)

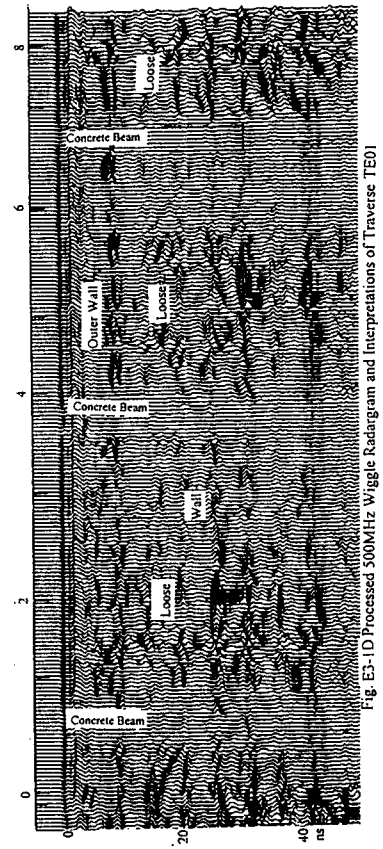

Fig. E3-1D Processed 500MHz Wiggle Radargram and Interpretations of Traverse TE01

E1b - After Institute of Geophysical & Geochemical Exploration (1996b)

Figure E1 - Examples of Radargrams Made Along Traverse TE01 at Site E Using 500MHz Antennas

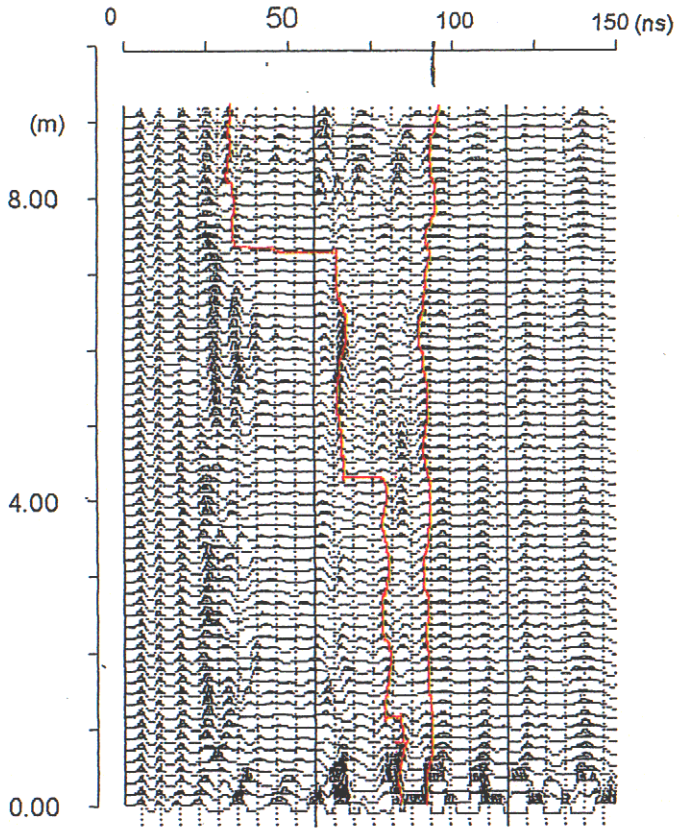

E2a - After Guandong South China EGDT Co. (1996b)

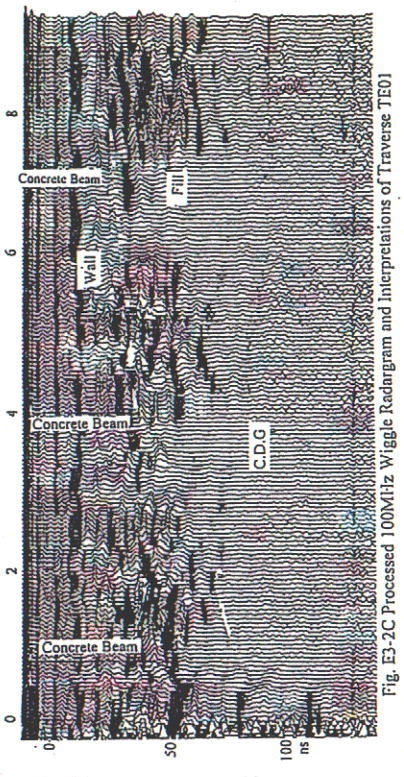

E2b - After Institute of Geophysical & Geochemical Exploration (1996b)

Figure E2 - Examples of Radargrams Made Along Traverse TE01 at Site E Using 100MHz Antennas

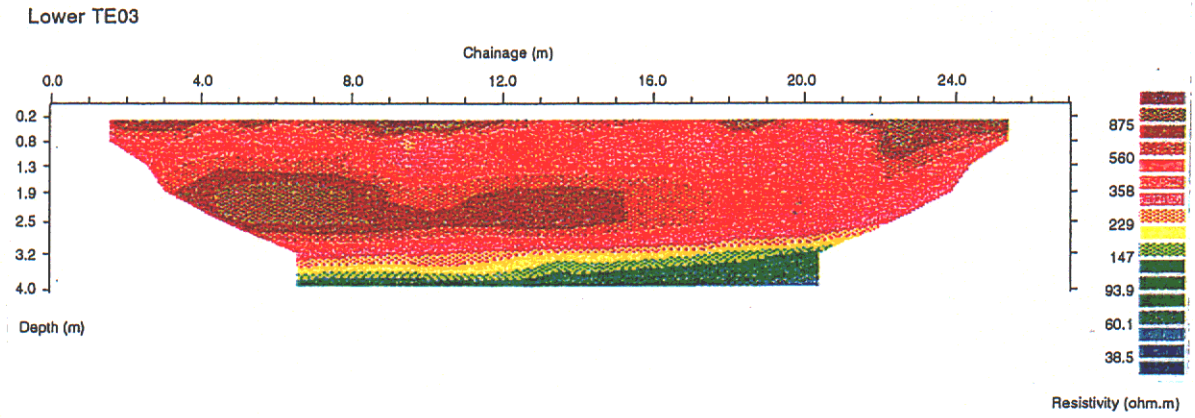

E3a - After Golder Associates (1996b)

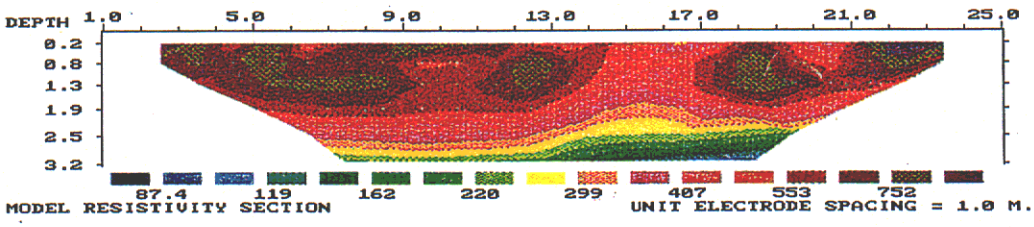

E3b - After Fugro Geotechnical Services (HK) Ltd (1996b)

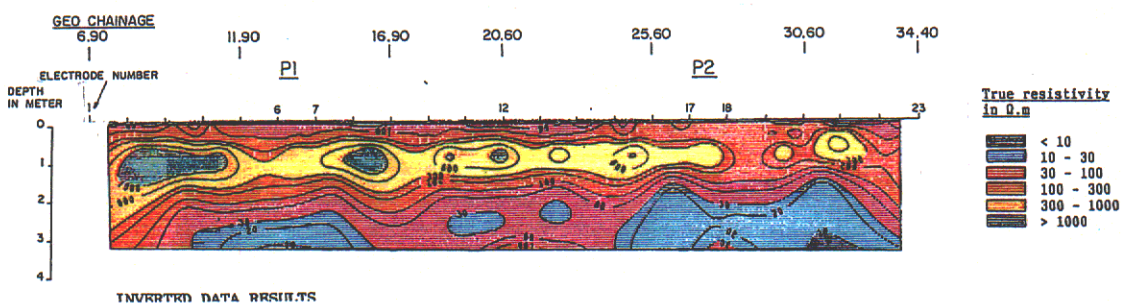

E3c - After Bachy Soletanche (1996b)

Figure E3 - Examples of Inverse Model Resistivity Sections Made Along TE03 at Site E

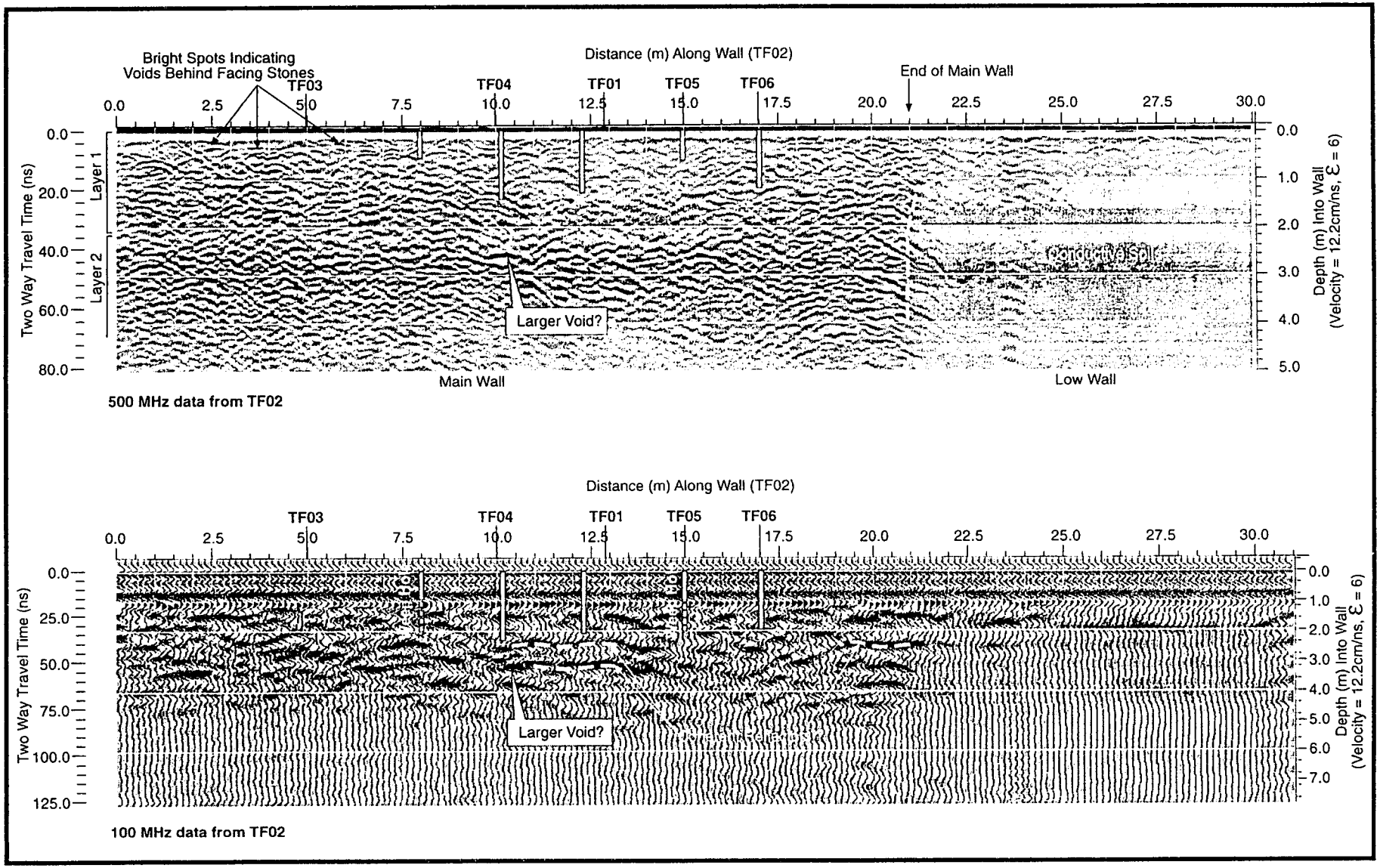

Figure E4 - Examples of 500MHz & 1000MHz Radargrams Made Along TF02 at Site F, after Golder Associates (1996b)

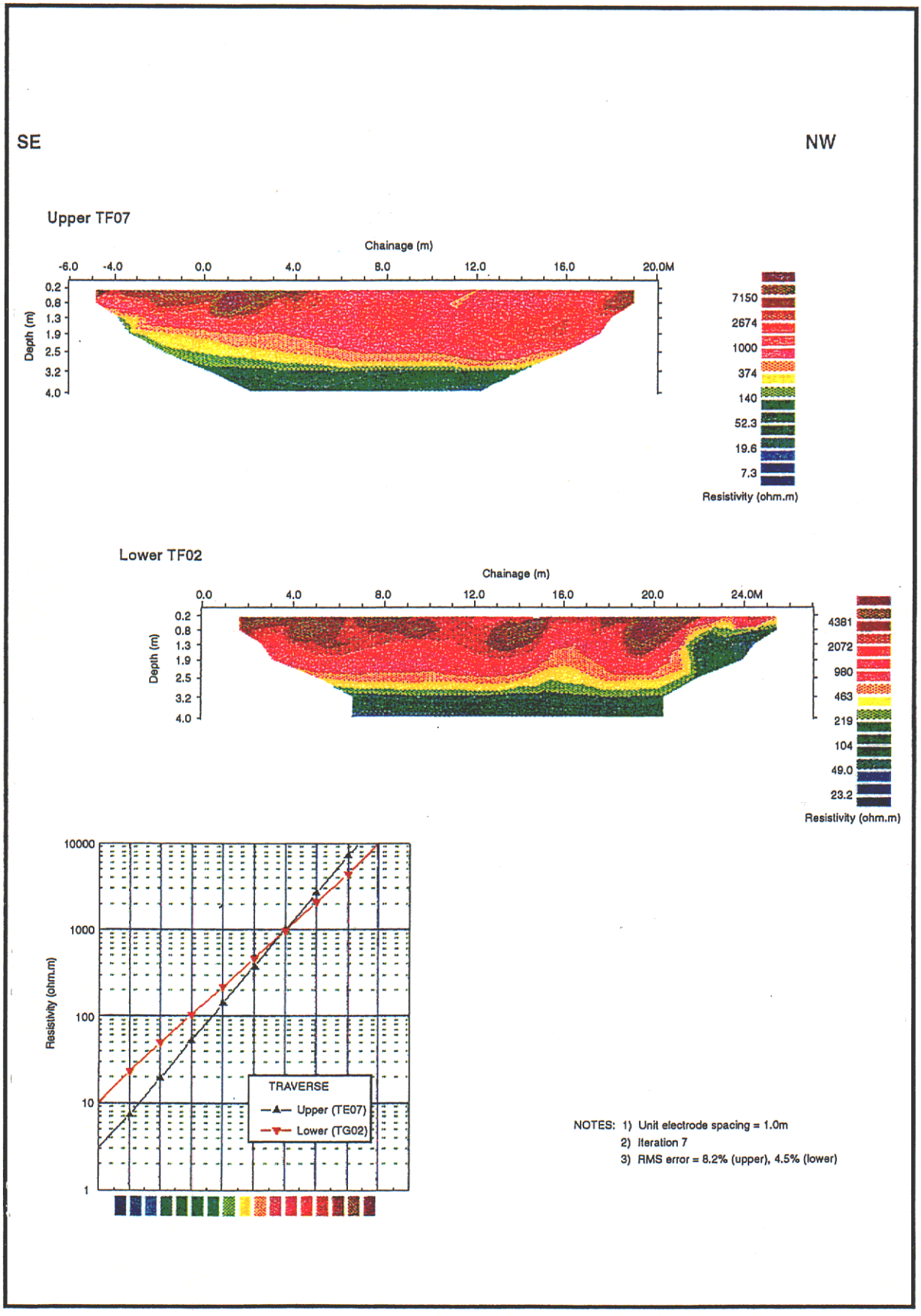

Figure E5 - Inverse Model Resistivity Sections Made Along TF02 and 2m above TF02 at Site F, after Golder Associates (1996b)

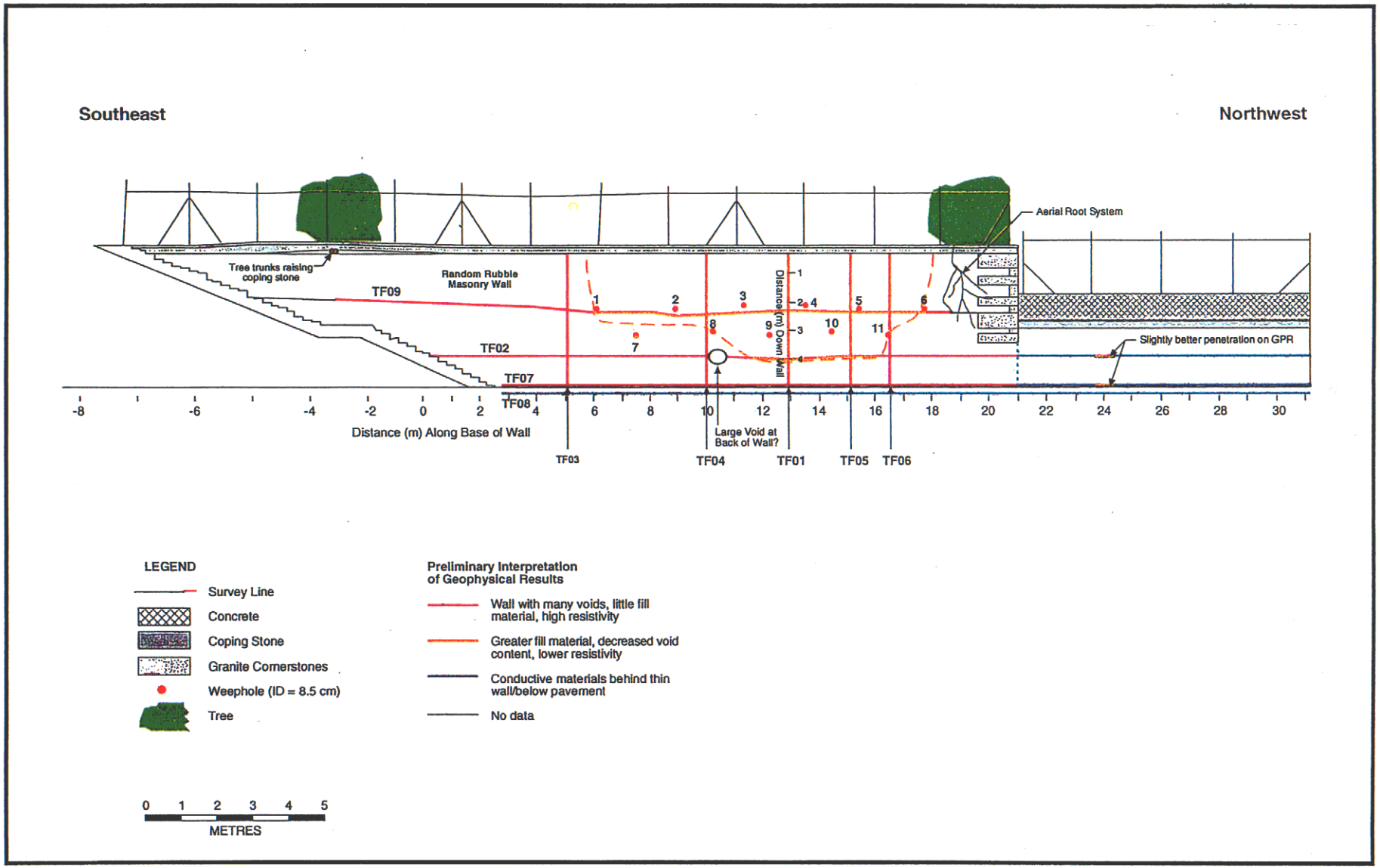

Figure E6 - Preliminary Interpretation of Anomalous Area within the Wall at Site F, after Golder Associates (1996b)

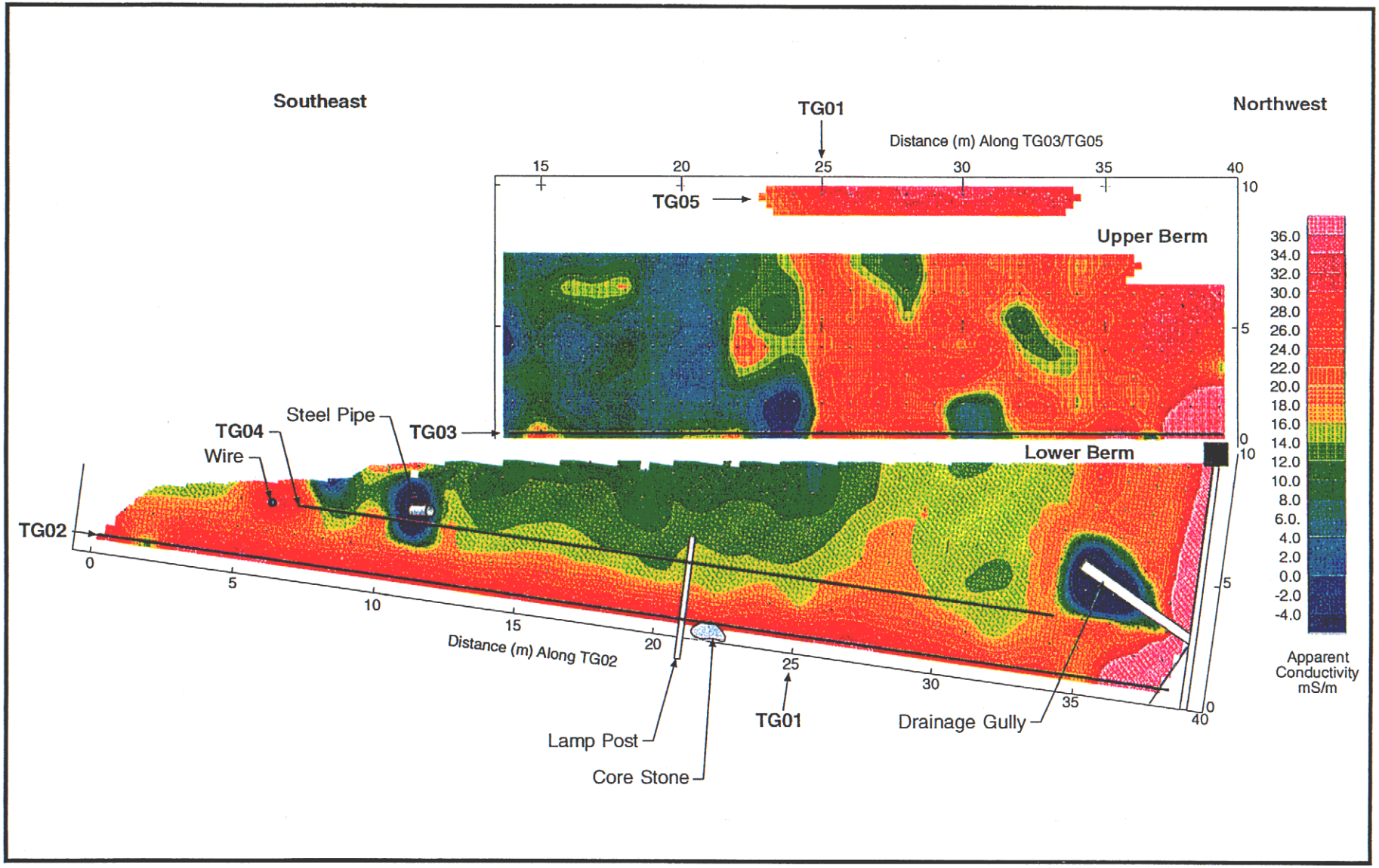

Figure E7 - Examples of Iso-conductivity Map Made Using the Geonics EM38 at Site G, after Golder Associates (1996b)

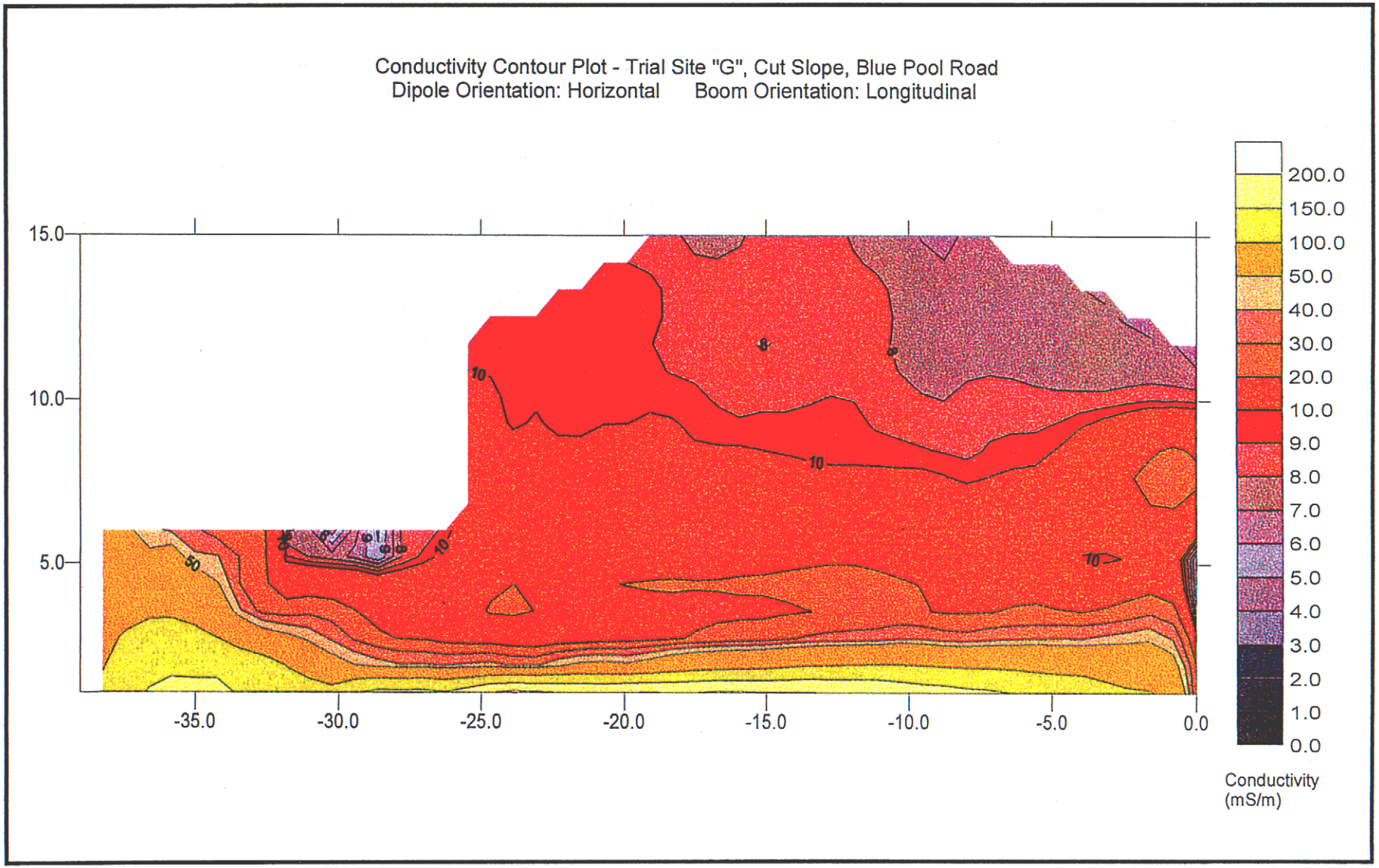

Figure E8 - Examples of Iso-conductivity Map Made Using the Geonics EM31 at Site G, after Fugro Geotechnical Services (HK) Ltd (1996b)

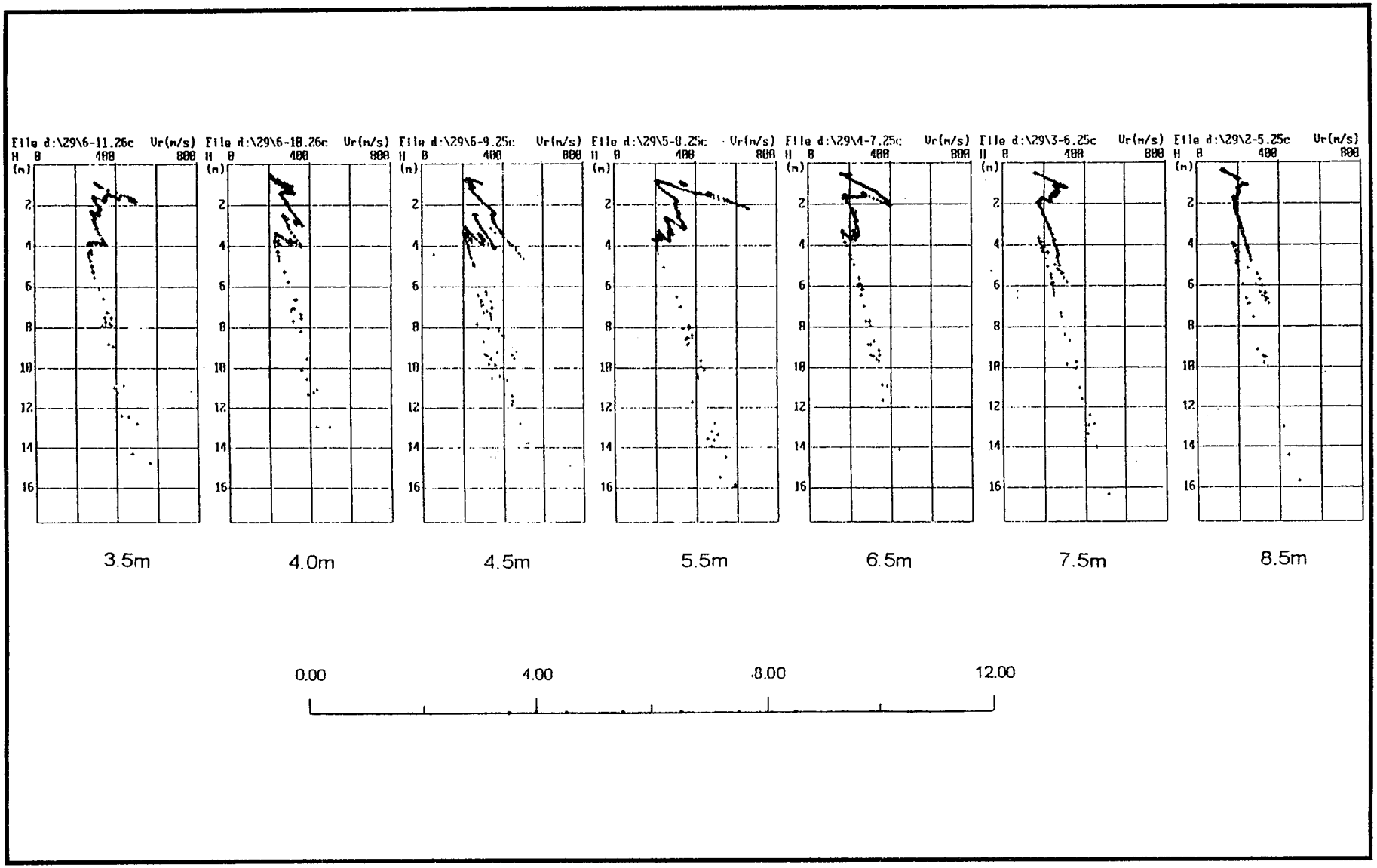

Figure E9 - Example of SASW Pseudo-dispersion Curves Made at Site H, after Guandong South China EGDT Co. Ltd (1996b)